A Grid Overlapping Scheme for Flowfield Computations About Multicomponent Configurations

Essam H. Atta* and Joseph Vadyak*
Lockheed-Georgia Company, Marietta, Georgia

An efficient grid interfacing zonal algorithm has been developed for computing the transonic flowfield about three-dimensional multicomponent configurations. The algorithm uses the full-potential formulation and the AF2 fully implicit approximate factorization scheme. The flowfield solution is computed using a component-adaptive grid approach in which separate grids are employed for the individual components in the multicomponent configuration, where each component grid is optimized for a particular geometry. The component grids are allowed to overlap, and flowfield information is transmitted from one grid to another through the overlap region. An overlapping grid scheme has been implemented for an isolated wing and a noninteracting wing/pylon/nacelle configuration. Numerical results show that the present algorithm is stable, accurate, and promises to be effective in computing the flowfield about complex configurations.

Introduction

RELIABLE and efficient three-dimensional transonic analysis methods are needed to make realistic and cost-effective predictions of aircraft aerodynamics. Early efforts to predict the transonic flowfield about aircraft multiple-component configurations are based on the transonic small-disturbance formulation.[1-3] This allows the geometry of the configuration to be greatly simplified and the surface boundary condition to be applied on a mean approximate surface. Accurate prediction of such flowfields, however, requires the use of the full-potential formulation and the generation of a suitable surface-fitted grid. Because each aircraft component (wing, nacelle, fuselage) requires, in general, a grid system that is usually incompatible with the grid systems of the other components, the generation of a single surface-fitted grid for the entire configuration is a difficult task. In such a global grid, control of grid point distribution, skewness, and clustering will be difficult to achieve. Efforts to predict the flowfield about a complete aircraft configuration using a single-grid approach have been made recently by Yu.[4]

In the present paper the alternate approach of using a component adaptive grid scheme is investigated. The basic idea of this approach is to develop a separate grid for each component of a complex configuration where each individual grid is optimized for a particular component. The flow solver for each component employs the AF2 fully implicit approximate factorization scheme.[5]

Earlier studies in two dimensions showed that by allowing the component grids to overlap, fast convergence can be achieved.[6] This approach has been generalized herein to three dimensions, where an overlapped grid scheme has been implemented for an isolated wing and a wing/pylon/nacelle configuration.

The application of an embedded grid scheme to an isolated wing geometry was performed primarily as a proof-of-concept study to verify the grid interfacing logic in three dimensions and to determine if single-grid results could be replicated. The application to the wing/pylon/nacelle configuration represents a more realistic use of the grid embedding technique. The full interacting algorithm has been tested for the isolated wing case. However, for the wing/pylon/nacelle configuration the algorithm has been tested for a noninteracting flowfield case where a converged isolated nacelle solution is imposed as fixed boundary conditions for an ensuing wing computation.

Presented as Paper 82-1017 at the AIAA/ASME Third Joint Thermophysics, Fluids, Plasma and Heat Transfer Conference, St. Louis, Mo., June 7-11, 1982; submitted July 16, 1982; revision received Nov. 22, 1982.

*Scientist, Advanced Flight Sciences Dept. Member AIAA.

Grid Generation

The basic idea underlying the present method is to employ an optimum grid for each component in the multicomponent configuration and then to interface the grids in a manner which allows for the efficient and accurate solution of the governing equations. Use of a separate body-fitted grid for each component greatly facilitates obtaining an accurate numerical solution, and circumvents the need for generating a single grid suitable for a complex multicomponent geometry.

An overlapped grid scheme has been used to implement the present method for an isolated wing and for a wing/pylon/nacelle configuration. The grid topologies for the isolated wing configuration are illustrated in Figs. 1-3. Figure 1 depicts the composite overlapped grid for the isolated wing. The overlapped grid is composed of an inner body-fitted curvilinear grid and an outer sheared Cartesian grid. The curvilinear inner grid is shown in isolation in Fig. 2 and is essentially identical to that used in the NASA Ames TWING transonic wing computer code[5] (a summary of pertinent computer codes employed in the present study is given in Table 1). This grid is obtained by generating a series of two-dimensional O-type grids for a number of spanwise wing stations. Each O-grid is obtained by solving a system of two coupled Laplace equations. The Cartesian outer grid is shown in isolation in Fig. 3 and is obtained using geometric stretching formulas in each of the three coordinate directions.

The grid topologies for the wing/pylon/nacelle configuration are illustrated in Figs. 4-7. A frontal view of the composite overlapped grid system is shown in Fig. 4. The outer grid is the wing grid and is generated for a series of spanwise stations starting at the symmetry plane and progressing past the wing tip. The inner grid is the nacelle grid and is generated for a series of meridional planes. (A meridional plane is a plane passing through the longitudinal axis of the nacelle.) Figure 5 shows a side view of the overlapped grid system at a particular spanwise station. The curvilinear outer wing grid, which is the O-type, is obtained using procedures identical to that employed for the isolated wing. Selected interior mesh points are deleted from the wing grid in order to accommodate the nacelle geometry as shown in Fig. 6. The curvilinear inner nacelle grid is of the C-type and

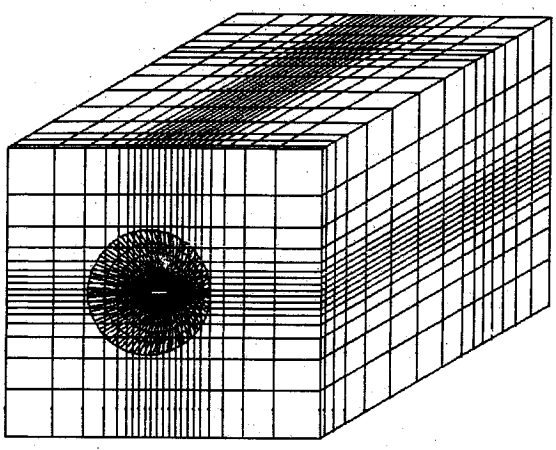

Fig. 1 Overlapped grid topology for isolated wing.

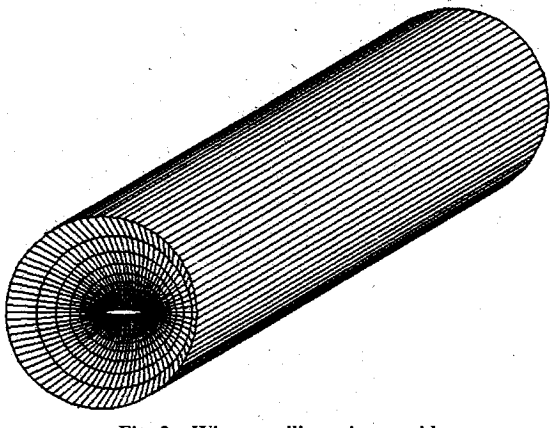

Fig. 2 Wing curvilinear inner grid.

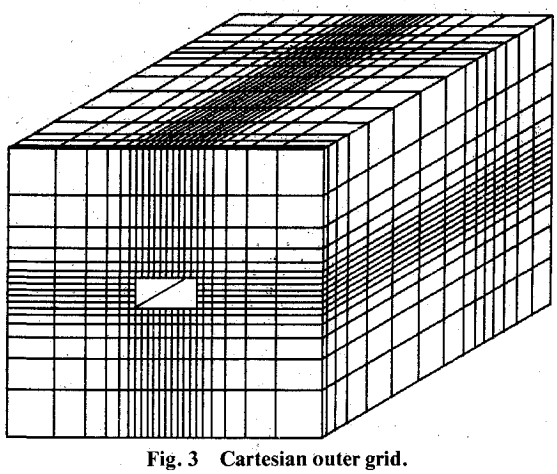

Fig. 3 Cartesian outer grid.

is generated for each meridional plane using a two-dimensional grid generation procedure. The grid generation procedure is applied only once for axisymmetric geometries, but is applied for each meridional plane in the case of asymmetric nacelle geometries. The NASA Ames GRAPE computer code[7] is used to generate the grid for a given meridional plane. The code generates a two-dimensional grid by solving two coupled Poisson equations. Each meridional plane grid is of the C-type and wraps around the nacelle hilite as shown in Fig. 7, which illustrates the nacelle grid in isolation.

Governing Equations

The governing equations for steady three-dimensional potential flow in an arbitrary curvilinear coordinate system

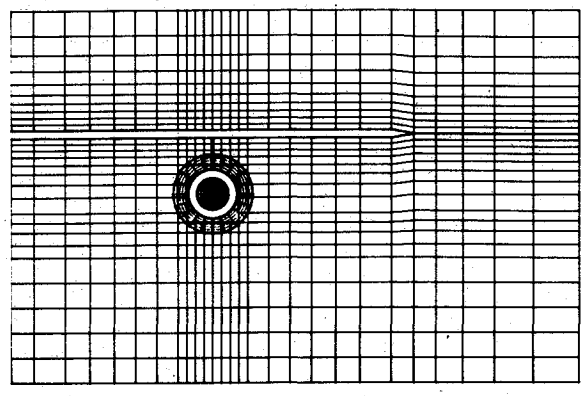

Fig. 4 Front view of overlapped wing/pylon/nacelle grid.

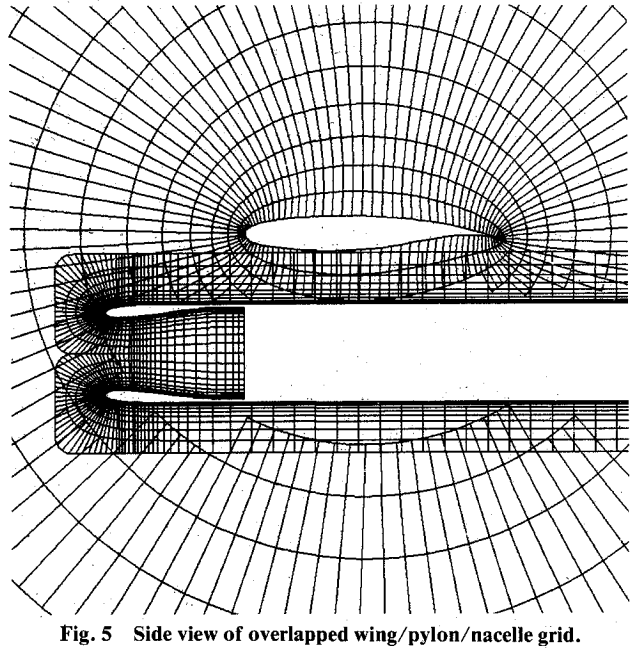

Fig. 5 Side view of overlapped wing/pylon/nacelle grid.

(ξ,η,ζ) are given by

$$\left(\frac{\rho U}{J}\right)_\xi + \left(\frac{\rho V}{J}\right)_\eta + \left(\frac{\rho W}{J}\right)_\zeta = 0 \tag{1}$$

$$\rho = \left[1 - \frac{\gamma-1}{\gamma+1}\left(U\phi_\xi + V\phi_\eta + W\phi_\zeta\right)\right]^{\frac{1}{\gamma-1}} \tag{2}$$

where U, V, W are the contravariant velocity components in the ξ, η, and ζ curvilinear coordinate directions, respectively; ρ is the density; J is the Jacobian of the transformation from a Cartesian coordinate system to the general curvilinear coordinate system (ξ,η,ζ); and γ is the specific heat ratio. The density and the contravariant velocity components are normalized by the stagnation density and the critical speed of sound, respectively. Equation (1) is the full-potential equation in strong conservation form and expresses mass continuity for three-dimensional steady flows. Equation (2) expresses entropy conservation and is used to determine the density ρ in terms of the velocity potential ϕ.

The contravariant velocity components U, V, and W can be expressed in terms of ϕ as

$$U = A_1\phi_\xi + A_4\phi_\eta + A_5\phi_\zeta \tag{3}$$

$$V = A_4\phi_\xi + A_2\phi_\eta + A_6\phi_\zeta \tag{4}$$

$$W = A_5\phi_\xi + A_6\phi_\eta + A_3\phi_\zeta \tag{5}$$

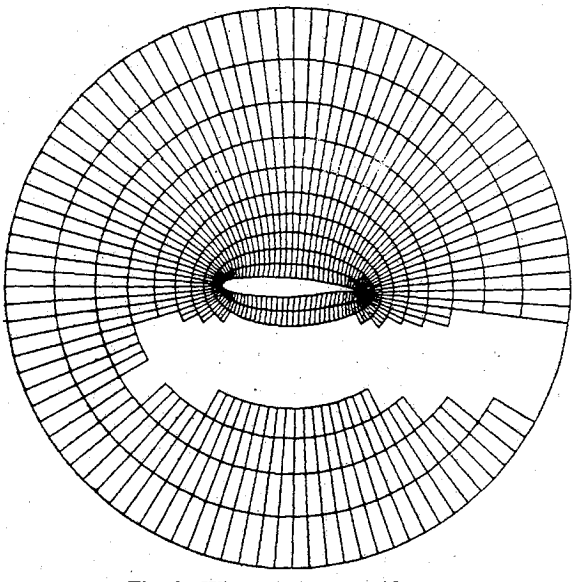

Fig. 6 Wing component grid.

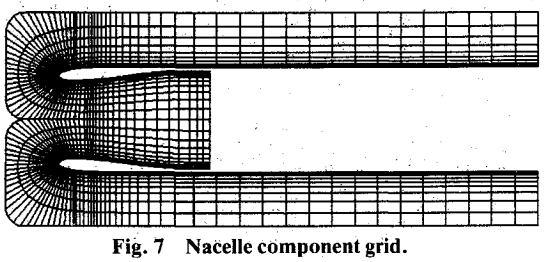

Fig. 7 Nacelle component grid.

Table 1 Summary of computer codes

Code	Usage	Developed by
GRAPE	Two-dimensional grid generation[a]	NASA Ames
TWING	Transonic full-potential wing analysis[a]	NASA Ames
FLO49	Transonic full-potential nacelle axisymmetric flow analysis[a]	Jameson
NACELLE	Transonic full-potential nacelle three-dimensional flow analysis[b]	Lockheed
TWPN	Transonic full-potential wing/pylon/nacelle analysis[b]	Lockheed

[a] = Developed. [b] = Under development.

Expressions for the metric parameters A_i and the Jacobian J are given by

$$A_1=\xi_x^2+\xi_y^2+\xi_z^2, \qquad A_2=\eta_x^2+\eta_y^2+\eta_z^2$$

$$A_3=\zeta_x^2+\zeta_y^2+\zeta_z^2, \qquad A_4=\xi_x\eta_x+\xi_y\eta_y+\xi_z\eta_z$$

$$A_5=\xi_x\zeta_x+\xi_y\zeta_y+\xi_z\zeta_z, \quad A_6=\eta_x\zeta_x+\eta_y\zeta_y+\eta_z\zeta_z \tag{6}$$

$$J=\xi_x\eta_y\zeta_z+\xi_y\eta_z\zeta_x+\xi_z\eta_x\zeta_y-\xi_z\eta_y\zeta_x-\xi_y\eta_x\zeta_z-\xi_x\eta_z\zeta_y \tag{7}$$

The metric parameters are computed using standard fourth-order accurate finite difference formulas.

Numerical Algorithm

The present numerical algorithm uses the finite difference formulation developed in Ref. 5. The full-potential equation is approximated by the finite difference expression

$$\overleftarrow{\delta}_\xi\left(\frac{\tilde{\rho}U}{J}\right)_{i+\frac{1}{2},j,k}+\overleftarrow{\delta}_\eta\left(\frac{\tilde{\rho}V}{J}\right)_{i,j+\frac{1}{2},k}+\overleftarrow{\delta}_\zeta\left(\frac{\hat{\rho}W}{J}\right)_{i,j,k+\frac{1}{2}}=0 \tag{8}$$

where i, j, k are the grid point indices in the ξ (wraparound), η (spanwise or circumferential), and ζ (normal) directions, respectively. The operators $\overleftarrow{\delta}_\xi(\ )$, $\overleftarrow{\delta}_\eta(\ )$, and $\overleftarrow{\delta}_\zeta(\ )$ are first-order backward difference operators in the ξ, η, and ζ directions, respectively. The terms $\tilde{\rho}$, $\bar{\rho}$, and $\hat{\rho}$ are upwind-biased density coefficients given by expressions of the form

$$\tilde{\rho}_{i+\frac{1}{2},j,k}=[(1-\nu)\rho]_{i+\frac{1}{2},j,k}+\nu_{i+\frac{1}{2},j,k}\rho_{i+\frac{1}{2}+r,j,k} \tag{9}$$

where r denotes an upwind point and ν is an artificial viscosity coefficient given by

$$\nu=0 \qquad \text{if } M_{i,j,k}<1$$

$$=C(M_{i,j,k}^2-1) \qquad \text{if } M_{i,j,k}>1 \tag{10}$$

where M is the local Mach number and C is a user-specified constant. Similar expressions hold for $\bar{\rho}$ and $\hat{\rho}$ which effect upwinding in the η and ζ directions, respectively.

The finite difference equations are solved using the AF2 approximate factorization scheme, which has proved to be significantly more efficient than successive-line-overrelaxation schemes. The AF2 algorithm is written in a three-step form as

Step 1:

$$\left(\alpha-\frac{1}{A_k}\vec{\delta}_\eta A_j\overleftarrow{\delta}_\eta\right)g_{i,j}^n=\alpha\omega L\phi_{i,j,k}^n+A_{k+1}f_{i,j,k+1}^n \tag{11}$$

Step 2:

$$\left(A_k\pm\beta_\xi\vec{\delta}_\xi-\frac{1}{\alpha}\vec{\delta}_\xi A_i\overleftarrow{\delta}_\xi\right)f_{i,j,k}^n=g_{i,j}^n \tag{12}$$

Step 3:

$$(\alpha+\overleftarrow{\delta}_\zeta)C_{i,j,k}^n=f_{i,j,k}^n \tag{13}$$

In Eqs. (11-13), α is a free parameter chosen to maintain stability and attain fast convergence, β_ξ is a factor that controls the amount of dissipation required in regions of supersonic flow, ω is a relaxation factor, n is the iteration number, $L\phi$ is the mass residual, f and g are intermediate functions obtained during the solution process, and C is the potential function correction given by

$$C_{i,j,k}^n=\phi_{i,j,k}^{n+1}-\phi_{i,j,k}^n \tag{14}$$

The terms A_i, A_j, and A_k are defined by

$$A_i=(\tilde{\rho}A_1/J)_{i-\frac{1}{2},j,k}^n \tag{15}$$

$$A_j=(\bar{\rho}A_2/J)_{i,j-\frac{1}{2},k}^n \tag{16}$$

$$A_k=(\hat{\rho}A_3/J)_{i,j,k-\frac{1}{2}}^n \tag{17}$$

In steps 1 and 2 the g and f functions are obtained by solving a tridiagonal system of equations, while in step 3 the correction C is obtained by solving a bidiagonal system of equations.

Boundary Conditions

For solid boundaries, such as the wing or nacelle surfaces, the tangency condition is implemented by setting the contravariant velocity component that is normal to the surface

equal to zero. For outflow boundaries, such as the compressor face inside the nacelle (see Fig. 7), the contravariant velocity component normal to the outflow surface is specified in terms of the nacelle mass flow ratio.

For the pylon surface, small disturbance boundary conditions are used. Freestream conditions are imposed at infinity. For the overlap region inner and outer boundaries, the velocity potential ϕ or the velocity potential normal derivative ϕ_n can be specified. Both options were tried in two dimensions[6] and no significant differences in the final results were observed. However, specifying the velocity potential, which is a scalar quantity, is easier to implement and requires less computational effort compared to specifying the velocity potential normal derivative.

Boundary conditions for the f and g intermediate functions on the overlap boundaries were selected, such that if ϕ is specified on these boundaries, f and g are set to zero, while if ϕ_η (normal derivative) is specified, then g_η and f_ξ are set to zero.

Iteration Procedure

As illustrated in Figs. 1 and 5, the component grids are allowed to overlap. For example, in the case of the wing/pylon/nacelle configuration, the inner bound for the wing component grid lies within the nacelle/inlet computational domain. Likewise, the outer bound for the nacelle/inlet component grid lies within the wing computational domain.

The computation is started by initializing the entire velocity potential field. Then the wing algorithm is executed for a specified number of iterations (typically 10) holding ϕ constant on the overlap inner boundary. The nacelle algorithm is then executed for a specified number of iterations using overlap outer boundary conditions as determined from the wing solution. At this stage, the wing algorithm is again executed using updated overlap inner boundary conditions obtained from the nacelle solution. This process is repeated until overall convergence is achieved. Typically 10 to 15 cycles are required for convergence.

Intergrid Property Transfer

Multivariate interpolation is employed to transfer property information between the component grids. To effect intergrid property transfer for the isolated wing configuration, a bivariate interpolation polynomial based on a quadratic Taylor series expansion was employed. Two-dimensional interpolation is possible in this case since the spanwise stations of the inner curvilinear grid and the outer Cartesian grid are selected to coincide. Interpolation is performed in computational (ξ, η, ζ) space using a polynomial of the form

$$f(\xi,\zeta) = f_0 + f_{\xi 0}(\xi-\xi_0) + f_{\zeta 0}(\zeta-\zeta_0) + \tfrac{1}{2}f_{\xi\xi 0}(\xi-\xi_0)^2 + \tfrac{1}{2}f_{\zeta\zeta 0}(\zeta-\zeta_0)^2 + f_{\xi\zeta 0}(\xi-\xi_0)(\zeta-\zeta_0) \quad (18)$$

where $f(\xi,\zeta)$ denotes the interpolated flow property at the point (ξ,ζ), and the subscript 0 denotes a selected interpolation base point in computational space. The derivatives appearing in Eq. (18) are evaluated using standard second-order accurate difference formulas. Point (ξ_0,ζ_0) is selected as the mesh point closest to the desired interpolation point (ξ,ζ).

The wing/pylon/nacelle configuration requires employing a trivariate interpolation polynomial since the component grids in this case do not have a common coordinate surface. A quadratic trivariate polynomial similar to Eq. (18) could be used for this application. However, to minimize the computation effort and to simplify the coding logic, the results presented herein for the wing/pylon/nacelle configuration employed a linear polynomial of the form

$$f(\xi,\eta,\zeta) = f_0 + f_{\xi 0}(\xi-\xi_0) + f_{\eta 0}(\eta-\eta_0) + f_{\zeta 0}(\zeta-\zeta_0) \quad (19)$$

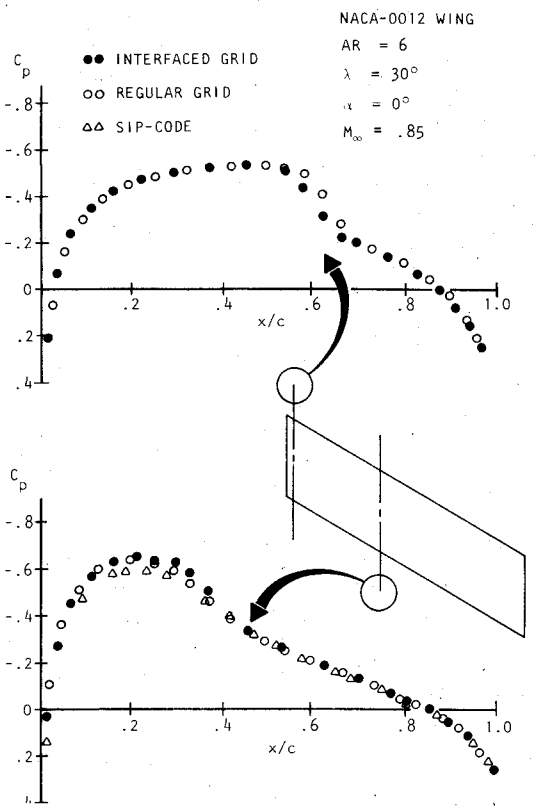

Fig. 8 Comparison of overlapped and single grid results for NACA 0012 wing.

Computed Results

The first step to implement the present scheme was to develop a code capable of solving the full-potential equation in a domain containing more than one grid system. Figure 1 shows a composite grid around a wing. The velocity potential is specified on the outer boundary of the inner surface fitted grid and on the inner boundary of the outer Cartesian grid. The NASA Ames full-potential wing code TWING[5] is modified and used as the flow solver for the inner grid. For the outer Cartesian grid, a full-potential code that solves the flow around box-type geometries was developed. Second-order, two-dimensional interpolation, as mentioned previously, was used to transfer the velocity potential values between the two grids during the iterative solution process. Performance of the present scheme was evaluated by comparing the results obtained by using the standard TWING code[5] and Lockheed-SIP transonic wing code.[8] Both of these codes use a single grid to solve for the transonic flow on a wing. Figure 8 gives a sample of the results obtained for a nonlifting NACA 0012 swept wing. The results are in good agreement. Because the inner curvilinear grid, which uses the major portion of the total computer time, is now localized in a small region of the flowfield, a 15% reduction in computer run time was obtained compared with the single grid code TWING. In the overlapped grid scheme, the inner boundary of the Cartesian grid is located one-half chord around the wing and the results were obtained using $101\times17\times11$ grid points for the curvilinear grid and $31\times17\times26$ points for the Cartesian grid. The TWING code solution was computed using $101\times17\times25$ grid points.

A wing/pylon/nacelle code (TWPN) that employs the present scheme was developed. This required the development of a three-dimensional nacelle code (NACELLE) and the modification of the NASA Ames TWING wing code to allow for the inclusion of the nacelle.

The overlapped grid topology for such a configuration is shown in Fig. 5. Presently, the pylon is treated as a vertical slit in the wing grid with small disturbance boundary conditions

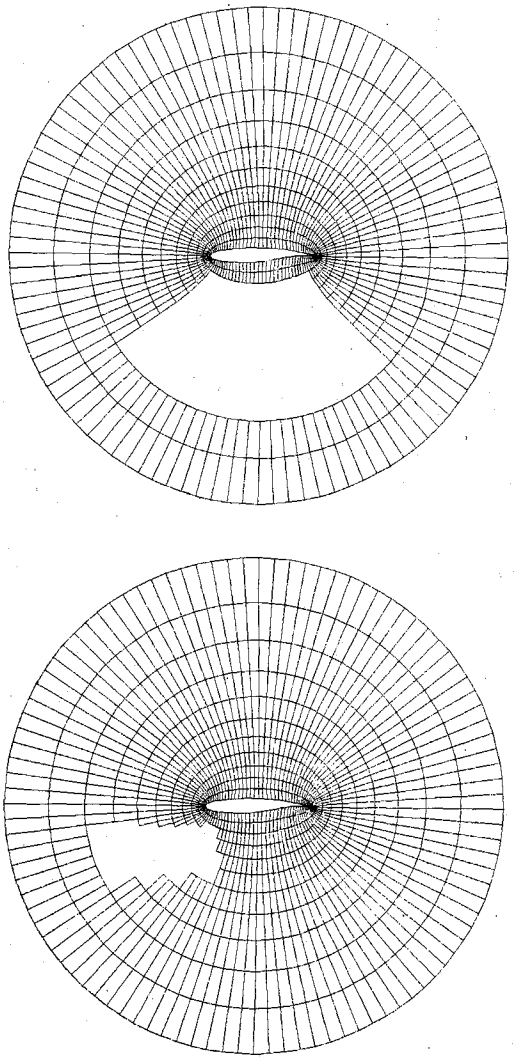

Fig. 9 Overlap boundary topologies.

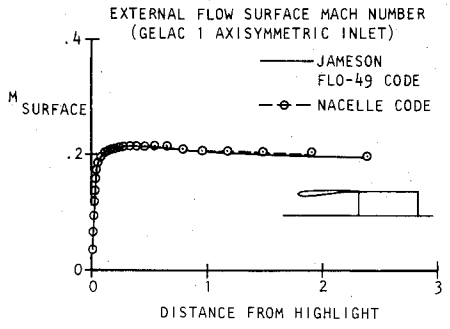

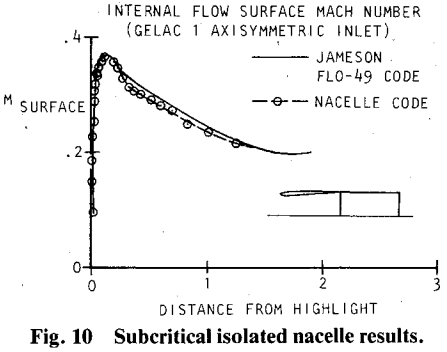

Fig. 10 Subcritical isolated nacelle results.

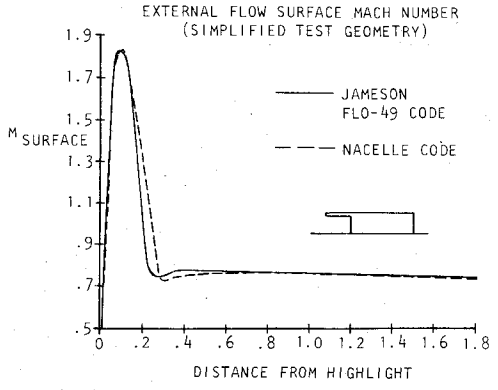

Fig. 11 Supercritical isolated nacelle results.

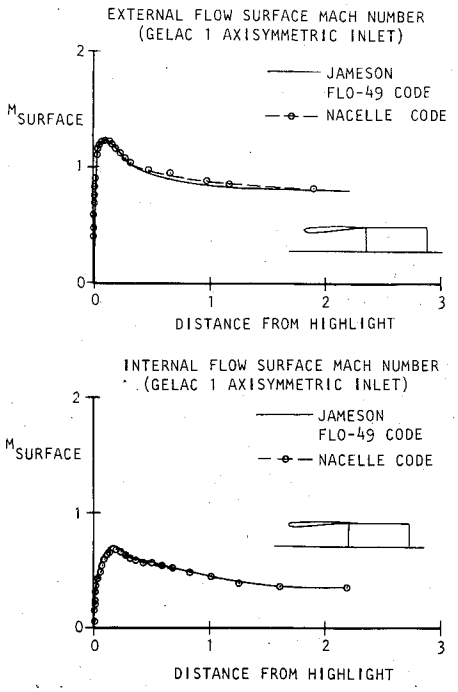

Fig. 12 Supercritical isolated nacelle results.

imposed on it. A separate grid for the pylon is currently under evaluation. Figures 6 and 7 show the wing and nacelle grids in isolation. The wing grid contains the overlap region inner boundary, while the nacelle grid outer boundary constitutes the overlap region outer boundary. The code is structured to allow for noninteracting or mutual interference run modes; that is, the velocity potential values that are imposed on the overlap region inner boundary in the TWPN code can be fixed or allowed to be updated during the solution process. The results presented in the present article are for the noninteracting case.

To check the code, a converged wing solution was obtained from the NASA Ames wing code TWING. The converged velocity potential values were used as boundary conditions for the overlap region inner boundary in the TWPN code. The code was then executed with different overlap boundary shapes (see Fig. 9), and in each case the converged wing flowfield solution was reproduced.

The three-dimensional nacelle code NACELLE is currently under development. However, computations were performed for two axisymmetric inlet configurations shown in Figs. 10-12 on relatively coarse grids. These calculations were performed using isolated nacelle grids similar to the one shown in Fig. 7, but which have their outer computational boundaries extended far enough to represent freestream conditions. Computed nacelle Mach number distributions for both in-

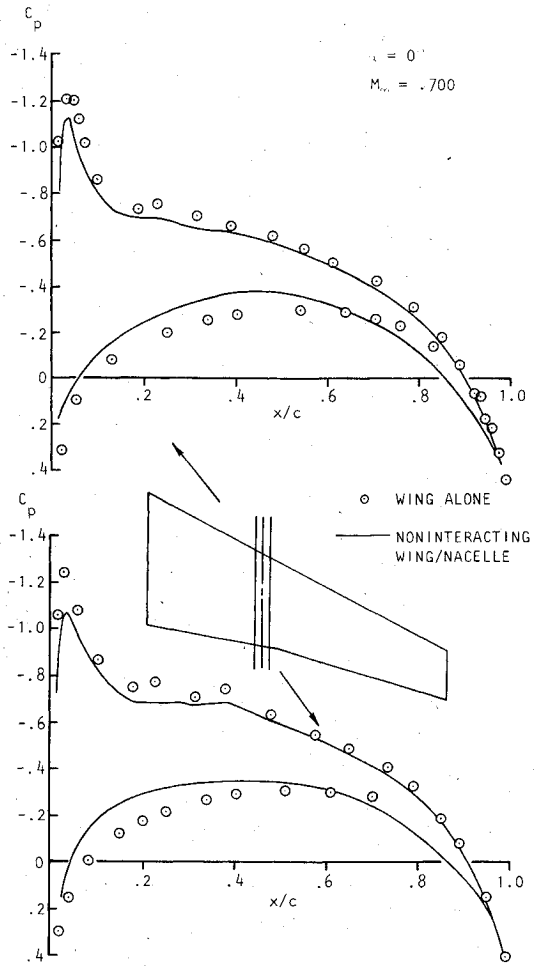

Fig. 13 Nacelle interference effect on wing pressure distribution.

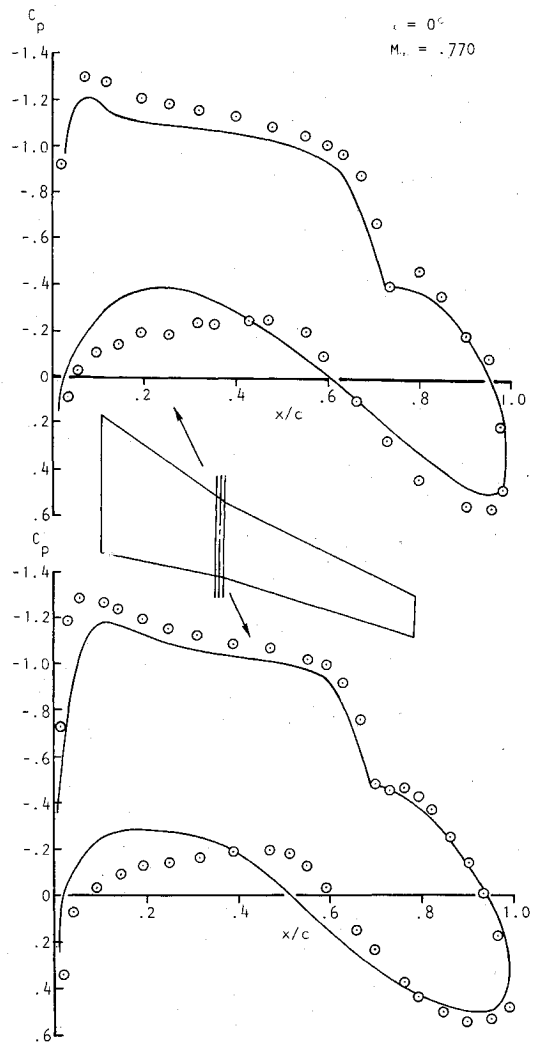

Fig. 14 Nacelle interference effect on wing pressure distribution.

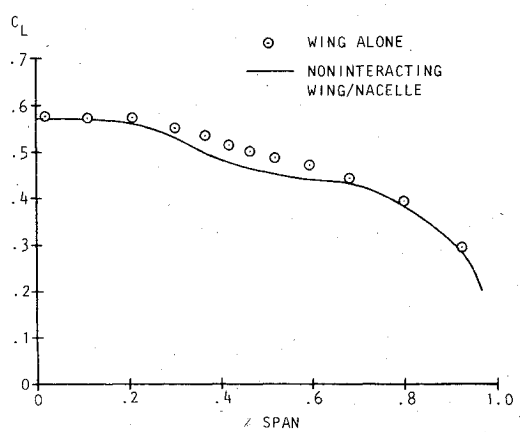

Fig. 15 Effect of nacelle on section lift coefficient.

ternal and external surfaces are illustrated. Also shown on these figures are the computed results of the Jameson FLO49 (Ref. 9) axisymmetric nacelle code. The FLO49 code is a two-dimensional, full-potential, finite-volume transonic nacelle code that uses the successive line overrelaxation scheme with multigrid convergence acceleration. The Mach number distributions produced by the two analyses agree very well. These results were performed on a 128×32 grid for the FLO49 code and a $66 \times 13 \times 13$ grid for the three-dimensional nacelle code.

To evaluate the performance of the TWPN code for noninteracting wing/nacelle flowfields, a converged nacelle solution was computed using the FLO49 code and imposed as boundary conditions for the overlap inner boundary. A linear Taylor series expansion, as mentioned previously, was used to interpolate the velocity potential from the FLO49 code grid system to the TWPN code grid system. The wing grid in the TWPN code employed $101 \times 26 \times 25$ grid points, while the FLO49 code used 128×32 grid points.

Figures 13-15 show the interference effect of the nacelle on two transport wing models. The pressure distributions are computed at 5% span inboard and outboard of the nacelle. The nacelle flowfield produced a marked change on the wing pressure distribution especially on the wing lower surface. This resulted in a loss of lift. These predictions agree qualitatively with the experimentally observed nacelle interference effect. A mutual interference solution should provide a more accurate prediction. The computations were performed on the VAX11/780 minicomputer and a typical noninteracting case requires about 2.5-3 h of CPU time.

Conclusions

An efficient grid interfacing zonal algorithm has been developed to compute the transonic flowfield about complex configurations. In the present method the difficult task of generating one global grid for a multicomponent configuration is replaced by the easier task of generating separate grids for each component. The optimized grid system produces the desired balance between convergence speed and accuracy of the flowfield solution. Numerical results using the overlapped grid scheme show that the present algorithm promises to be very effective in computing the flowfield about multicomponent configurations.

Acknowledgments

This work was supported in part by the NASA Ames Research Center under Contract NAS2-11285 and in part by

the Lockheed-Georgia Company. The authors also wish to express their appreciation to Ms. K. Hall of Southern Technical Institute and Mr. G. Shrewsbury of Lockheed-Georgia Company.

References

[1] Boppe, C. W. and Stern, M. A., "Simulated Transonic Flows for Aircraft with Nacelles, Pylons, and Winglets," AIAA Paper 80-0130, 1980.

[2] Shankar, V. and Malmuth, N. D., "Computational and Simplified Analytical Treatment of Transonic Wing-Fuselage-Pylon Store Interactions," AIAA Paper 80-0127, 1980.

[3] Srokowski, A. J., Shrewsbury, G. A., and Lores, M. E., "A Transonic Mutual Interference Program for Computing the Flow about Wing/Pylon/Nacelle Combinations," AIAA Paper 80-1333, 1980.

[4] Yu, N. J., "Transonic Flow Simulation for Complex Configurations with Surface Fitted Grids," AIAA Paper 81-1258, 1981.

[5] Holst, T. and Thomas, S., "Numerical Solution of Transonic Wing Flow Fields," AIAA Paper 82-0105, 1982.

[6] Atta, E. H., "Component-Adaptive Grid Interfacing," AIAA Paper 81-0382, 1981.

[7] Sorensen, R. L., "A Computer Program to Generate Two-Dimensional Grids about Airfoils and Other Shapes by Use of Poisson's Equation," NASA TM-81198, 1980.

[8] Sankar, N. L., Malone, J., and Tassa, Y., "A Strongly Implicit Procedure for Steady Three-Dimensional Transonic Potential Flows," *AIAA Journal*, Vol. 20, May 1982, pp. 598-605.

[9] Jameson, A., "Transonic Flow Analysis for Axially Symmetric Inlets With Center Bodies," Antony Jameson and Associates, Inc., Princeton, N.J., Rept. No. 2, 1981.